Diurnal modulation of multivesicular release controls the efficiency of information transmission at a sensory synapse

José Moya-Díaz, Ben James, Federico Esposti, Jamie Johnston and Leon Lagnado*

Sussex Neuroscience, School of Life Sciences, University of Sussex,
Brighton BN1 9QG, UK

*Corresponding author: l.lagnado@sussex.ac.uk

Summary

Sensory circuits adapt to changes in the external world or the animal's internal state through the actions of neuromodulators[1,2]. Synapses are key sites at which neuromodulators act[3,4] but it is not known how they alter the amount of information transmitted[5]. We investigated this question in the context of the diurnal regulation of visual processing in larval zebrafish, focusing on ribbon-type synapses of retinal bipolar cells[6]. We demonstrate that contrast-sensitivity peaks in the afternoon accompanied by an average four-fold increase in the Shannon information transmitted at individual active zones. This increase reflects higher synaptic gain, lower spontaneous "noise", reduced variability of stimulus-evoked release and improved temporal precision. Simultaneously, an increase in the probability of multivesicular events with larger information content increases the efficiency of information transmission (bits per vesicle) by factors of 2-3. The neuromodulator dopamine contributes to all these changes in synaptic function, although ON and OFF visual channels are differentially affected. Multivesicular release is a property of synapses in many parts of the brain[7-11] and this study demonstrates that it's potentiation by neuromodulators can both increase the amount of information that is transmitted and the efficiency of transmission, revealing a previously unknown mechanism for adjusting neural processing.

It has long been understood that the flow of signals through neural circuits is adjusted by neuromodulators[1]. Less clear is how these alter the amount of information that is transmitted through the circuit[3]. Here we investigate this question in the context of visual processing in the retina.

In diurnal animals, the sensitivity of the retina to light is regulated both by the daily light-dark cycle and by intrinsic circadian clocks[12-15]. But the average luminance of a visual scene is not the variable driving most behaviours related to vision: navigation, finding food and avoiding predators all depend on detection of fast modulations in light intensity. We therefore investigated the diurnal control of temporal contrast processing, focusing on the visual signal transmitted by glutamatergic synapses of bipolar cells. These neurons are the bridge between the photoreceptors and ganglion cells that deliver the results of retinal processing to downstream circuits[6]. The synaptic compartments of bipolar cells contribute to a number of processing tasks, from adaptive gain control to temporal filtering and the coding of motion, colour, orientation and direction[6,16-20]. Bipolar cells, like sensory hair cells and electroreceptors, contain ribbon structures that supply vesicles to the active zone[21]. These sensory synapses do not always operate as Poisson machines in which vesicles are released independently but also signal through multivesicular release (MVR), where the fusion of two or more vesicles is co-ordinated as a single synaptic event[8,22,23]. MVR is also a common property of neocortical[9,11], striatal[10] and cerebellar[24] synapses.

Diurnal modulation of contrast-sensitivity and synaptic gain

Using SyGCaMP2[25] we found that synaptic calcium responses to modulations in light intensity varied during the day and peaked in the subjective afternoon (Fig. 1A-D). At ZT = 4 hours, temporal contrasts below 50% were barely detected and the half-maximal response ($C_{1/2}$) was generated by a stimulus contrast of 86 ± 2 % (red

traces in Figs. 1B-C). But at ZT = 7 hours $C_{1/2}$ it fell to 35 ± 2 % with responses saturated above 50%. When $C_{1/2}$ was mapped during the course of the day it was relatively constant at ZT 1-5 hours and ZT 9-14 hours but increased to levels ~2.4-fold lower around ZT = 7 hours (Fig. 1D). Notably, this peak in the contrast sensitivity of the retinal circuit occurred at a similar *Zeitgeber* time as the maximum contrast sensitivity measured behaviourally using the optokinetic reflex[13,15]. Luminance sensitivity was also under diurnal control but with a distinctive time-course, gradually increasing ~200-fold through the day (Extended Data Figure 1).

To measure transmission of the visual signal in terms of its elementary units – synaptic vesicles - we expressed the reporter iGluSnFR sparsely in bipolar cells[23,26] (Fig. 1E; see Methods and Extended Data Figure 2). Synaptic function was compared over a two-hour period beginning 1 hour after light onset ("morning") with a two-hour period beginning 6 hours later ("afternoon"; Fig. 1F). We began by measuring the contrast-response function (CRF) simply as the average number of vesicles released per cycle of a 5 Hz stimulus. There was notably little diurnal modulation of the CRF measured at ON synapses (Fig. 1H) but in the OFF channel the maximum rate of release measured at 100% contrast increased from 3.05 ± 0.5 vesicles/s in the morning to 5.1 ± 0.3 vesicles/s in the afternoon (Fig. 1G). This increase in synaptic gain was also accompanied by an increase in contrast sensitivity ($1/C_{1/2}$) and the combined effects were assessed as the derivative of the CRF ("contrast gain"; Fig. 1I). Contrasts in natural visual scenes rarely exceed 40%[17] and in the morning this range was signalled best through the ON channel. But in the afternoon the OFF channel became dominant, with contrast gains increasing by factors of 2-6.

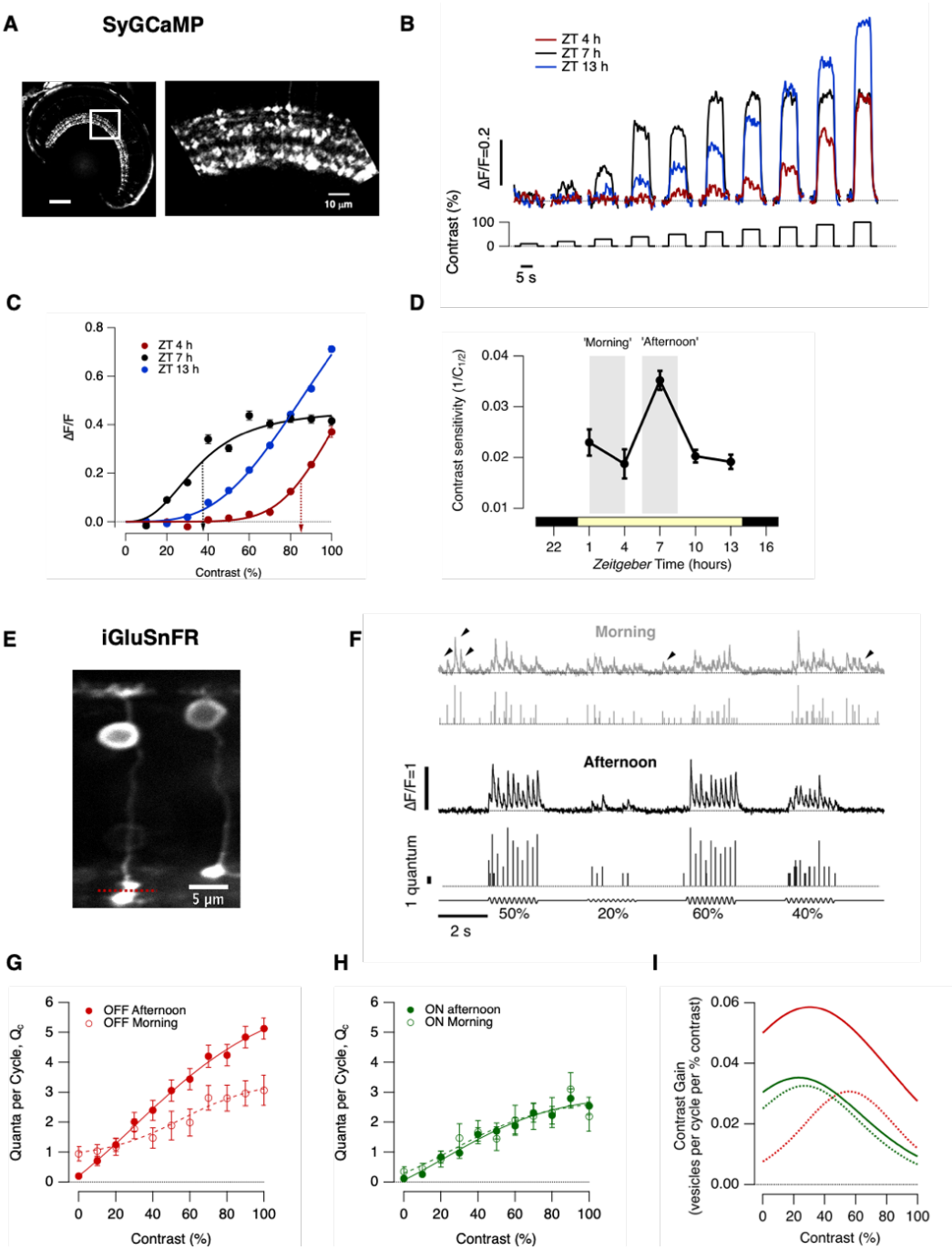

Figure 1: Diurnal modulation of contrast-sensitivity and synaptic gain

A. Left: Retina of a Ribeye::SyGCaMP2 fish with box over the IPL. Right: expansion of the boxed region of showing terminals of bipolar cells. **B.** Averaged responses to stimuli of different contrasts measured at *Zeitgeber* time 4, 7 and 13 hrs. **C.** Peak response amplitude as a function of contrast for terminals shown in B. The smooth lines are Hill functions used to interpolate values of $C_{1/2}$, the contrast generating the half-maximal response. Note the diurnal variations. At ZT = 4 hrs: $C_{1/2}$ = 86 ± 2% (dashed red arrow); h = 7.0 ± 1.2. At ZT = 7 hrs: $C_{1/2}$ = 35 ± 2% (dashed black arrow); h = 2.7 ± 0.2. At ZT = 13 hrs: $C_{1/2}$ = 72 ± 2%; h = 3.3 ± 0.2. **D.** Variations in contrast-sensitivity as a function of *Zeitgeber* time averaged across ON and OFF terminals. Note the peak around ZT = 7 hours which is not mirrored in the diurnal variation in luminance sensitivity (Extended Data Figure 1). The grey bars

show the periods described as "morning" and "afternoon". All error bars show ± 1 SD. **E**. Multiphoton section through the eye of a zebrafish larva (7 dpf) expressing iGluSnFR in a subset of bipolar cells. The red dashed line shows the typical position of a line-scan through a synaptic terminal. **F**. Examples of iGluSnFR signals from an individual OFF synapse elicited using a stimulus of variable contrast modulated at 5 Hz (0-100%, full field, sine wave) in the morning (ZT 1-3 hours, grey) and afternoon (ZT 6-9 hours, black). Note the high levels of spontaneous activity in the morning (black arrowheads). In each case the top trace shows the iGluSnFR signal and the lower trace the estimated number of quanta composing each event (Q_e). **G.** Average contrast-response functions in OFF bipolar cell synapses in the morning (open circles; n = 20 synapses) and afternoon (closed; n = 59), where the response (*R*) was quantified as the average of quanta per cycle (Q_c). The smooth lines are fits of a sigmoid used for smoothing. Note the differences in the shape of the contrast-response functions and in the levels of spontaneous activity (zero contrast). **H.** Average contrast-response functions in ON bipolar cell synapses in the morning (open circles; n = 12 synapses) and afternoon (closed; n = 31). There was no significant difference in in the morning relative to afternoon (Chi-square test, p = 0.9999). **I.** The contrast gain calculated as the derivative of the fits to the contrast-response functions in G and H. Note that the maximum contrast discrimination is increased by a factor of 2x in the OFF channel during the afternoon.

Dopamine regulates contrast gain

A key neuromodulator in the retina is dopamine released from amacrine cellsunder control of internal circadian clocks[12,27] as well as external signals, such as changes in luminance[14] or the appearance of food-related odours[28]. Dopamine levels are a minimum at night and increase throughout the day to modulate luminance-sensitivity[14,29] (Extended Data Figure 3). To test whether dopamine also regulates contrast sensitivity we injected agonists or antagonists of D1 receptors into the eye. Fig. 2A shows examples of the output from a synapse imaged in the afternoon, before and after injection of the D1 antagonist SCH 23390 (~0.1 μM). Counteracting the actions of endogenous dopamine reduced the average rate of vesicle release and shifted the CRF such that the maximum contrast gain was achieved at higher contrasts (Fig. 2B and C). Conversely, increasing activation of D1 receptors in the morning by injection of the agonist ADTN (~0.2 μM) increased response gain.

The dynamic range over which D1 receptors adjusted synaptic gain was calculated as the ratio of the CRFs in the presence of the agonist and antagonist: in both ON and OFF channels the maximum modulation was ~16-fold, occurring at

contrasts of 20-40% (Fig. 2D). Diurnal modulation of gain was narrower than this potential range: 1.7-fold in OFF synapses and 1.1-fold in ON.

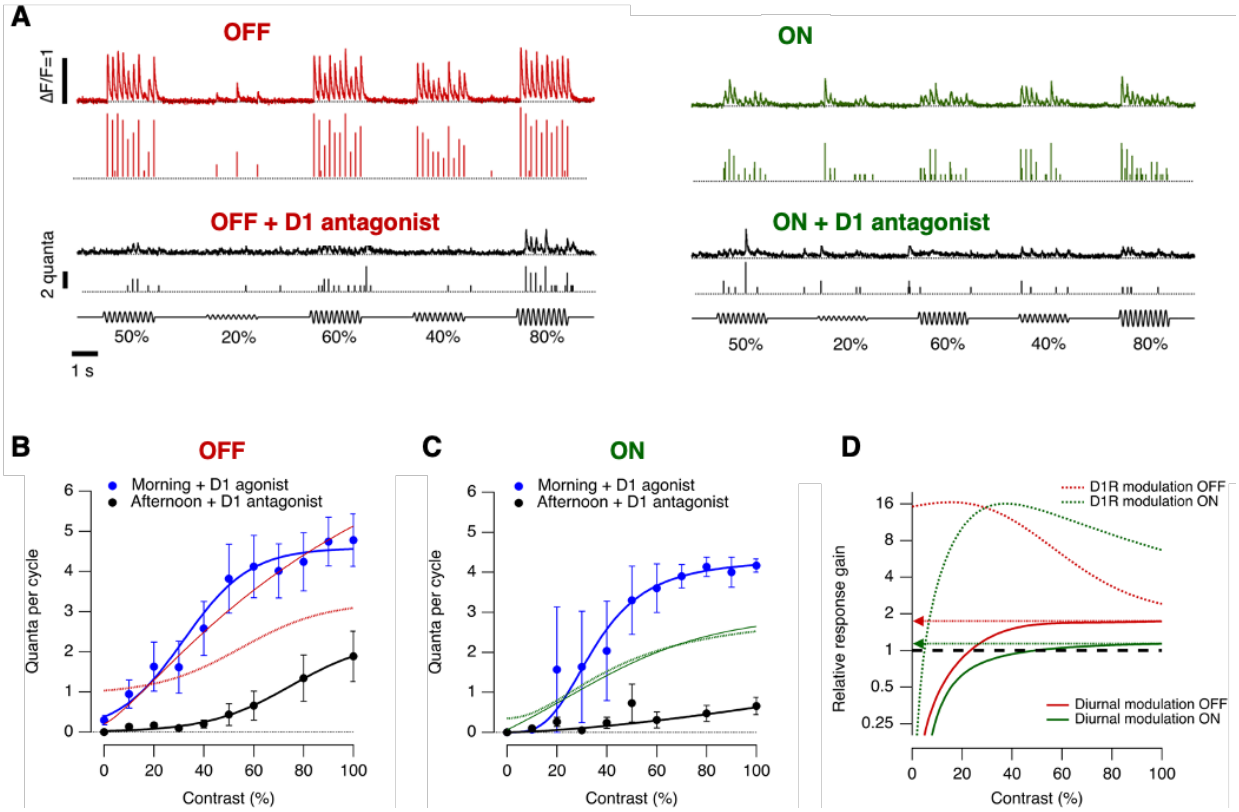

Figure 2. Diurnal changes in dopamine levels modulate of contrast-sensitivity and synaptic gain
A.Examples of iGluSnFR signals recorded in the afternoon from an individual OFF (red trace) and ON (green trace) synapses elicited using a stimulus of variable contrast before and after intravitreal injection of the D1 antagonist, SCH 23390 (black traces; 5 Hz modulation). Note that SCH 23390 abolished synaptic responses at lower contrasts in ON and OFF synapses. In each case the top trace shows the iGluSnFR signal and the lower trace the estimated Q_e. **B.** Average contrast-response functions in OFF bipolar cell synapses after administration of D1 antagonist (black dots) in the afternoon and after administration of the D1 agonist ADTN in the morning (blue dots). Each point shows the mean ± s.e.m. (SCH 23390, n =12 synapses; ADTN, n = 12 synapses). Control responses observed in the morning and afternoon are superimposed in the graph (red lines, see Fig. 2C) **C.** Average contrast-response functions in ON bipolar cell synapses in three conditions: afternoon (green dots), after intravitreal injection of D1 antagonist in the afternoon (black dots) and ADTN in the morning (blue dots). Each point shows the mean ± s.e.m. (SCH 23390, n =7 synapses; ADTN, n = 5 synapses). Control responses observed in the morning and afternoon are superimposed to the graph (green lines, see Fig. 2D). **D**. Relative response gain by diurnal modulation and after manipulation of dopaminergic signalling (dashed lines). Note that diurnal modulation of synaptic gain is higher in OFF synapses, whereas dopamine modulates the dynamic range by ~16 fold-change in ON and OFF synapses.

154 **Diurnal modulation of synaptic noise and variability**

155 In the framework of information theory[30], an increase in synaptic gain will tend to
156 reduce uncertainty (and therefore increase information) by causing a larger change
157 in the number of vesicles released when contrast changes. But information is
158 destroyed by "noise" and synapses are a major source of such variability within
159 neural circuits[5,31,32]. We therefore investigated the diurnal modulation of four
160 aspects of synaptic noise and variability.

161

162 ***i) Spontaneous release.*** Increases in synaptic gain were accompanied by a
163 *decrease* in the spontaneous release of vesicles in the absence of a visual stimulus.
164 In the morning, spontaneous events occurred at relatively high rates (Fig. 3A)
165 composed of both single vesicles and MVR (Fig. 3B and C). Integrating across
166 events of all amplitudes, the average rate of spontaneous release in OFF synapses
167 was 4.5 ± 2.5 vesicles s^{-1} in the morning falling to 1 ± 0.2 vesicles s^{-1} in the afternoon
168 (Fig 3B). In ON synapses these values were 1.8 ± 0.8 vesicles s^{-1} and 0.5 ± 0.2
169 vesicles s^{-1} (Fig. 3C). In both channels, therefore, spontaneous noise was ~4 times
170 lower in the afternoon compared to the morning. Increased activation of D1
171 receptors suppressed noise in the morning to levels close to those measured in the
172 afternoon, but only in OFF synapses (Fig. 3B and C).

173

174

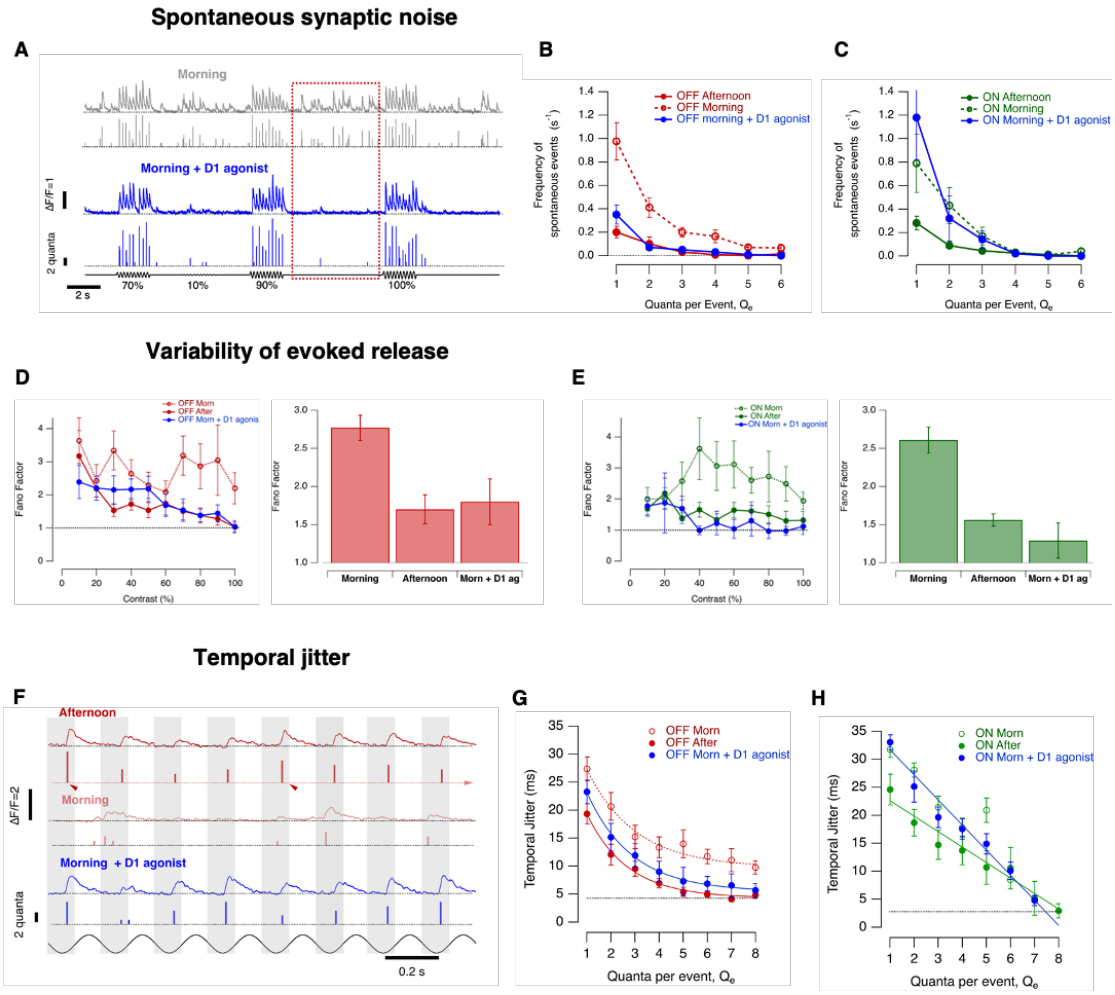

175

176 **Figure 3. Diurnal modulation of synpatic noise and variability**

177 **A.** *Top:* Example of iGluSnFR signals from an individual OFF synapse elicited using a stimulus of
178 variable contrast in the morning (0-100%, 5 Hz modulation). In this example, note the high levels of
179 spontaneous activity that were quantified as the responses elicited at zero contrast (red dashed box)
180 . *Bottom.* Examples of iGluSnFR signals from the same OFF synapse after intravitreal injection of
181 ADTN. Note the increase in amplitude and frequency of events and the reduction of spontaneous
182 activity. In each case the top trace shows the iGluSnFR signal and the lower trace the estimated Q_e.
183 **B.** Quantification of spontaneous events composed by different Q_e in OFF synapses in the morning (n
184 = 20 synapses), morning + ADTN (n = 12) and afternoon (n = 24 synapses). Note the suppression of
185 spontaneous events in OFF synapses after intravitreal injection of ADTN in the morning. **C.** As B, but
186 in ON synapses (n = 5-17). Spontaneous activity was not significantly changed by ADTN. **D.** Left:
187 Variability in the evoked response of OFF synapses calculated as the Fano factor, where each
188 response was quantified as the total number of vesicles released over one cycle at the contrasts
189 shown. Comparison is made between the morning (n = 18), afternoon (n = 27) and the morning after
190 injection of ADTN (n = 13). Right: Average Fano factor for each condition was significantly higher in
191 the morning compared to ether the afternoon or in the morning after injection of ADTN (t-test;
192 $p<0.0001$; bars ± 1 sd). **E**. As in D, but for ON synapses (n = 12, 15 and 6 synapses for respective
193 conditions). Again, the average Fano factor was significantly higher in the morning (t-test; $p<0.001$).
194 **F.** Example recordings from two OFF synapses stimulated at 60% contrast in three conditions:

afternoon (top, deep red trace), morning (middle, rlight red trace) and after injection of ADTN in the morning (bottom, blue trace). The comparison with and without ADTN is from the same synapse. In each case the top trace shows the iGluSnFR signal and the lower trace the estimated Q_e. The modulation in intensity is shown below. Note that events occur at different phases of the stimulus. **G.** Temporal jitter of events composed of different numbers of quanta in OFF synapses in the afternoon (n = 24 synapses), morning (n = 19) and morning + ADTN (n = 16). Release events occurring in the morning were significantly less phase-locked than the afternoon ($p<0.001$; t-test). Activation of D1 receptors reduced temporal jitter for events composed of 3 or more quanta ($p < 0.004$). The solid lines describing these relations in the three conditions are described by a single exponential decay function of the form $y_0 + A_{exp}((-(x-x_0)/\tau)))$ with y0= 4.23 ± 1.2 and A = 27 ± 7 in the afternoon; y0= 9.77 ± 1.4 and A= 28.64 ± 5.6 in the morning and y0=5.45 ± 1.3, A = 30. ± 6.1 after activation of D1 receptor in the morning. **H**. As G, but for ON synapses (n = 6-14). Activation of D1 receptors had no significant effect on temporal jitter. The relationship observed in the morning is described by a straight line with a = 34.7 ± 1.5 and a slope = -3.6 ± 0.5.

ii) Variability in stimulus-evoked responses. This was assessed by the Fano factor (F), the ratio of the variance-to-mean of the response measured over multiple trials[33,34]. In the morning, F was ~2.6 in both ON and OFF synapses when averaged over a range of contrasts, falling to ~1.6 in the afternoon ($p < 0.001$, t-test; Fig.3D-E). Notably, the variability of synaptic output was higher than expected for a Poisson process, for which F = 1. Activation of D1 receptors in the morning improved the reliability of synaptic responses to levels similar to those measured in the afternoon (Fig.3 D-E).

iii) Temporal jitter. Retinal ganglion cells (RGCs) encode information not just in their spike count but also in the timing of spikes[35,36]. Spike times can vary by just a few milliseconds and this accuracy depends on the precision of excitatory inputs received from bipolar cells[37]. The standard deviation in timing of release events ("temporal jitter") was measured relative to the phase of a 5 Hz stimulus and the larger the release event the more precise it was on average (Fig. 3F-H). In OFF synapses the temporal jitter was 5-8 ms lower in the afternoon compared to the morning for events composed of up to 8 vesicles (Fig. 3G). Diurnal modulation of temporal precision was weaker in ON synapses and only significant for events

228 composed of 1-3 vesicles (Fig. 3H). Increasing activation of D1 receptors in the
229 morning reduced temporal jitter in OFF synapses ($p < 0.004$, t-test) but not ON.
230
231 ***iv) Changes in the distribution of multivesicular events.*** Previous studies
232 quantifying the synaptic transfer of visual information have been limited by the
233 inability to monitor individual active zones and used the assumption that vesicles are
234 released according to Poisson statistics[38-40]. We know now that bipolar cells do not
235 employ a simple rate-code and that visual information is also contained in the
236 *amplitude* of multivesicular events[23]. To test whether modulation of contrast gain
237 was accompanied by changes in the number of quanta in an event (Q_e) we
238 compared the amplitude distribution in the morning and afternoon. Fig. 4A makes
239 this comparison for a stimulus of 60% contrast. In ON synapses, 68% of release
240 events in the morning were univesicular, falling to 40% in the afternoon ($p < 10^{-4}$,
241 chi-squared test) and this shift was fully reversed by antagonizing D1 receptors (Fig.
242 4B). MVR was more prevalent in OFF synapses with only 38% of release events in
243 the morning being univesicular but again there was a significant shift towards MVR
244 in the afternoon (Fig. 4C; $p<0.02$). Qualitatively similar diurnal modulation of MVR
245 was observed over a range of contrasts from 20% to 80%.
246
247

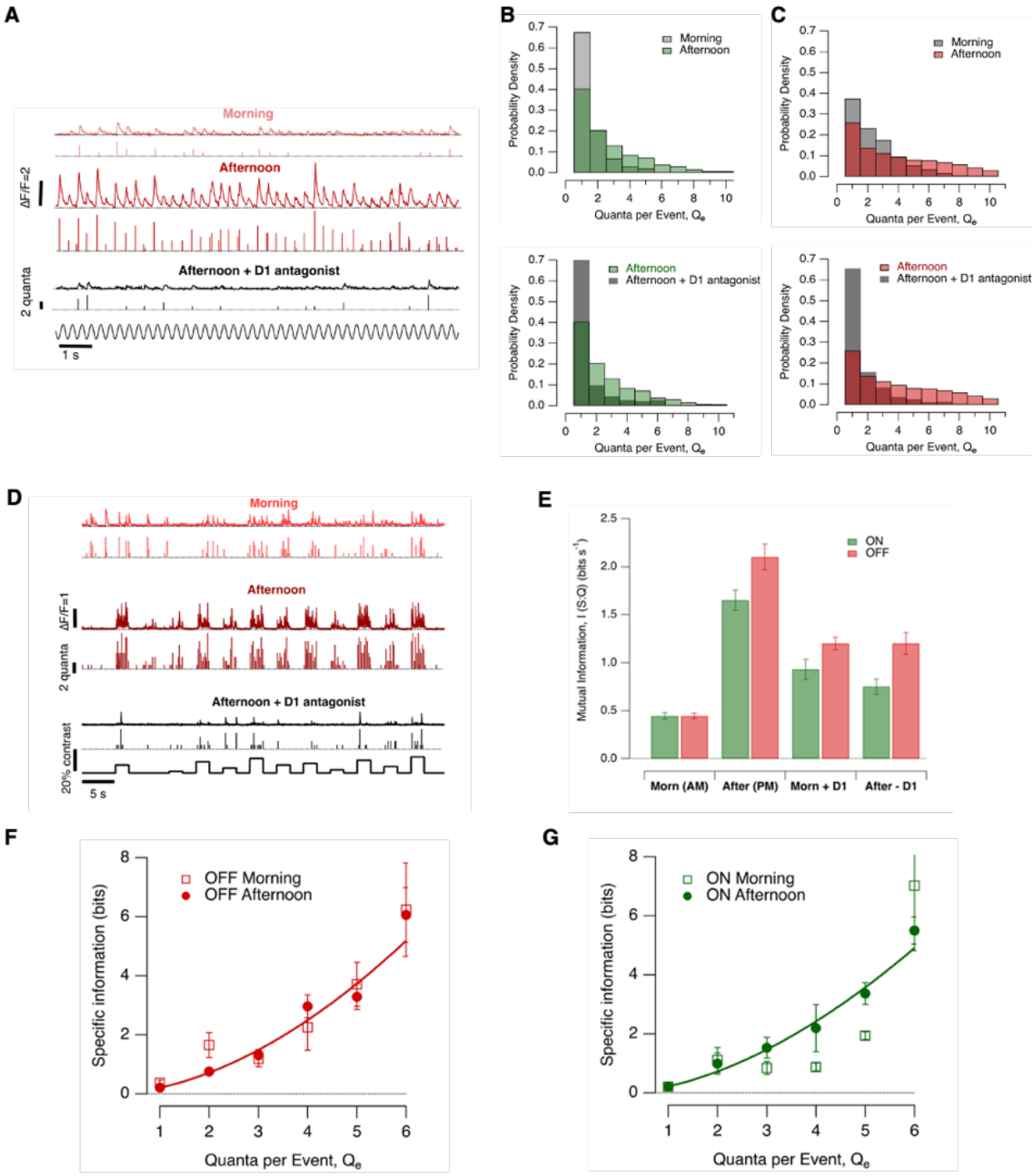

Figure 4. Diurnal changes in the efficiency of information transmission

A. Examples of iGluSnFR signals from an individual synapse elicited (60% contrast, 5 Hz) in the morning, afternoon and afternoon after injecting SCH 23390. In each case the top trace shows the iGluSnFR signal and the lower trace the estimated Q_e. **B**. Top: Changes in Q_e in ON synapses in the morning and afternoon. In the afternoon the distribution was shifted toward multiquantal events ($p<0.059$, Chi-squared test). Bottom: Changes in the distribution of Q_e in ON synapses before and after intravitreal injection of the D1 antagonist SCH23390. The distribution was shifted toward lower Q_e ($p<0.001$) but was not significantly different to that measured in the morning. **C.** As B, but for OFF

synapses. In the afternoon the distribution was shifted toward multiquantal events ($p<0.007$). In the afternoon, injection of SCH 23390 shifted the distribution toward uniquantal events ($p<0.001$). **D.** Examples of synaptic responses over 12 different contrasts spanning ±10% around the contrast eliciting the half-maximal response ($C_{1/2}$) in the morning (top, light red), afternoon (middle, dark red) and after injection of D1 antagonist SCH 23390 in the afternoon (bottom, black; note the lower frequency and amplitude of release events). In each case the top trace shows the iGluSnFR signal and the lower trace the estimated Q_e. Each contrast step lasted 2 s (5 Hz) and each trace is from a different OFF synapse. **E.** Mutual information *I (S;Q)* in four conditions: (i) morning, (ii) afternoon, iii) morning after injection of ADTN, (iv) afternoon after injection of SCH 23390. **F.** Specific information (I_2) for events of different quantal content in OFF synapses (33 synapses). The curve describing the relation is a least-squares fit of a power function of the form $i = AQ_e^x$, with $A = 0.20$, and $x = 1.81$. **G.** As F, but for ON synapses (n = 13). The curve describing the relation is almost identical ($A = 0.21$, and $x = 1.75$).

Diurnal modulation of information transmission

How do changes in synaptic gain (Figs.1-2), noise and variability (Fig. 3) and MVR (Fig. 4-C) combine to alter the amount of visual information transmitted? A larger synaptic signal relative to noise (SNR) will increase the mutual information (I) between the response (q) and the stimulus generating it (S), although the size of the increase will depend on the statistical properties of both signal and noise[41]. In the simple situation where both have a Gaussian distribution $I = 0.5\log_2(1+SNR)$[42]. But how should we quantify the synaptic signal? When analyzing the spike code, all events comprise the same symbol and the response can be described as the number of spikes in each of a series of time bins[41,43]. The output from bipolar cells is qualitatively different with a visual stimulus being encoded both by the timing of release events and their amplitudes[23]. We therefore took an approach in which MVR composed of different numbers of vesicles were considered different symbols. The mutual information between the response and stimulus was then computed as the average amount of information about the stimulus gained from observing any symbol[30,44].

In the morning, the average mutual information between stimulus and response was almost the same for ON and OFF synapses (0.445 ± 0.035 bits s^{-1} and 0.455 ±

0.03 bits s^{-1}, respectively; Fig. 4E). In the afternoon mutual information increased through both channels but the increase in OFF synapses (370%) was significantly larger than in ON (270%; $p < 0.001$ by t-test; Fig. 4E). Mutual information in the morning was increased by activation of D1 receptors and in the afternoon it was decreased by antagonizing the effects of endogenous dopamine, although not to levels measured in the morning (Fig. 4E).

Together, the results in Figs. 1-4 demonstrate that dopamine is a key neuromodulator controlling diurnal changes in information transmission in the retina, but also leave open the possibility that other pathways contribute.

Diurnal changes in the efficiency of the vesicle code

The transmission of information using spikes and vesicles requires energy so an important question becomes the efficiency with which these symbols are used[45]. RGCs firing at low rates cells transmit ~3.5 bits/spike while those that fire most briskly encode ~2 bits/spike[46]. In comparison, the 2.7-fold increase in information transmitted through ON synapses in the afternoon (Fig. 4E) occurred *without* a change in the average rate of vesicle release (Fig. 2D and E). In OFF synapses, mutual information increased 3.7-fold while release rates around $C_{1/2}$ increased just 2-fold (Fig. 2C and E). The diurnal increase in the average rate of vesicle release was therefore associated with a 1.4- to 2.7-fold *increase* in the average efficiency with which vesicles were used to encode changes in contrast. This situation is distinct to that observed in the binary spike code of post-synaptic RGCs, where an increase in spike rate is associated with a *decrease* in the efficiency of information transmission[46].

How does the vesicle code become more efficient at higher average release rates? To understand this we need to consider changes in the distribution of vesicles: MVR events become more prevalent in the afternoon (Fig. 4A-C) and

larger MVR events carry more information per vesicle[23], as shown by the supralinear relation between the specific information carried by each synaptic symbol and the number of vesicles it contains (Fig. 4F-G). This relation did not, however, change in the afternoon compared to the morning, at least for events composed of 1-6 vesicles (Fig. 4F and G; chi-squared test). The amount of information carried by each synaptic symbol was therefore independent of diurnal changes in visual processing.

Discussion

Synapses allow the flow of information through circuits to be adjusted[1,5] and this study provides a quantitative understanding of this idea in the context of the diurnal control of sensory processing. We find a dopamine-dependent increase in transmission of visual information that can be ascribed to four major effects: an increase in the number of vesicles released by a stimulus (Figs. 1 and 2), a decrease in spontaneous noise (Fig. 3A-C), reduced variability of evoked responses (Fig. 3D-H) and a shift from univesicular to multivesicular release (Fig. 4). The relative contributions of these various mechanisms differed between ON and OFF pathways but MVR was fundamental to both.

A recent combination of electrophysiology with correlative light-and electron-microscopy has led to the suggestion that it may be a fundamental mode of synaptic transmission throughout the nervous system[11] and it is established that MVR can be modulated by activity[7,47] and by presynaptic modulation, for instance through muscarinic acetylcholine receptors in the striatum[10] or $GABA_B$ receptors in the cortex[48]. This study has demonstrated that potentiation of MVR can not only increase the amount of information that a sensory synapse transmits but also increases the efficiency with which it is transmitted. Ever-improving techniques for monitoring synaptic output *in vivo* will help us understand how far neuromodulators

342 acting in other parts of the brain modulate MVR and the vesicle code that transmits
343 information between neurons.
344
345
346 # Methods
347
348 **Zebrafish husbandry**
349 Fish were raised and maintained under standard conditions on a 14 h light/10 h dark
350 cycle[40]. To aid imaging, fish were heterozygous or homozygous for the casper mutation
351 which results in hypopigmentation and they were additionally treated with1-phenyl-2-
352 thiourea (200 μM final concentration; Sigma) from 10 hours post fertilization (hpf) to
353 reduce pigmentation. All animal procedures were performed in accordance with the
354 Animal Act 1986 and the UK Home Office guidelines and with the approval of the
355 University of Sussex Animal Welfare and Ethical Review Board. More information
356 about experimental design and reagents is available in the Life Sciences reporting
357 Summary.
358
359 **Transgenic fish**
360 Experiments were carried out using the following transgenic lines of zebrafish:
361 i) *Tg(ribeye:;Zf-SyGCaMP2)* expressing the synaptically-localized fluorescent
362 calcium reporter SyGCaMP 2.0 in retinal bipolar cells under the ribeye-A promoter[25].
363 *ii) Tg(–1.8ctbp2:Gal4VP16_BH)* fish that drive the expression of the transcriptional
364 activator protein Gal4VP16 were generated by co-injection of I-SceI meganuclease
365 and endofree purified plasmid into wild-type zebrafish with a mixed genetic background.
366 A myocardium-specific promoter that drives the expression of mCherry protein was
367 additionally cloned into the plasmid to allow for phenotypical screening of founder fish.

iii) Tg(10xUAS:iGluSnFR_MH) fish driving the expression of the glutamate sensor iGluSnFR under the regulatory control of the 10 x UAS enhancer elements were generated by co-injection of purified plasmid and tol2 transposase RNA into offspring of AB wildtype fish outcrossed to casper wildtype fish. The sequences for the myocardium-specific promoter driving the expression of enhanced green fluorescent protein (mossy heart) were added to the plasmid to facilitate the screening process.

iv) *Tg(–1.8ctbp2:SyGCaMP6)* fish were generated by co-injection of I-SceI meganuclease and endofree purified plasmid into wild-type zebrafish with a mixed genetic background. The GCaMP6f variant was kindly provided by L. Looger (Janelia Farm). This variant holds a T383S mutation in comparison to the commercially available GCaMP6-fast version (Addgene plasmid 40755).

v) *Tg(isl2b:nlsTrpR, tUAS:memGCaMP6f)* which drives the expression of memGCaMP6f in the optic tectum was generated by co-injecting pTol2-isl2b-hlsTrpR-pA and pBH-tUAS-memGaMP6f-pA plasmids into single-cell stage eggs. Injected fish were out-crossed with wild-type fish to screen for founders.

Multiphoton Imaging *In Vivo*

Experiments were carried out in a total of 117 zebrafish larvae (7–9 days post-fertilization). Fish were immobilized in 3% low melting point agarose (Biogene) in E2 medium on a glass coverslip (0 thickness) and mounted in a chamber where they were superfused with E2. Imaging was carried out using a two-photon microscope (Scientifica) equipped with a mode-locked titanium-sapphire laser (Chameleon, Coherent) tuned to 915 nm and an Olympus XLUMPlanFI 20x water immersion objective (NA 0.95). To prevent eye movements, the ocular muscles were paralyzed by injection of 1 nL of α-bungarotoxin (2 mg/mL) behind the eye. Most imaging was carried out in the dorsal the retina.

The signal-to-noise ratio of the microscope was optimized by collecting photons through both the objective and a sub-stage oil condenser (Olympus, NA 1.4). Emission was filtered through GFP filters (HQ 535/50, Chroma Technology) before detection with GaAsP photomultipliers (H7422P-40, Hamamatsu). The signal from each detector passed through a current-to-voltage converter and then the two signals were added by a summing amplifier before digitization. Scanning and image acquisition were controlled under ScanImage v.3.6 software[49]. In iGluSnFR recordings images were acquired at 10 Hz (128 × 100 pixels per frame, 1 ms per line) while linescans were acquired at 1 kHz. In GCaMP recordings images were acquired at 20 Hz (128 × 50 pixels per frame, 1 ms per line). Full-field light stimuli were generated by an amber LED (I_{max} = 590 nm, Thorlabs), filtered through a 590/10 nm BP filter (Thorlabs), and delivered through a light guide placed close to the eye of the fish. These wavelengths will most effectively stimulate red and green cones. The microscope was synchronized to visual stimulation.

Stimulation protocols

Measurements of contrast sensitivity with SyGCaMP2 were made by stimulating the fish with a series of 10 s stimuli (full-field sinusoidal modulation at 5 Hz) around a mean intensity of 55 nW $mm^{-2.}$ Measurements of contrast sensitivity with iGluSnFR used 2 s stimuli. To measure the distribution of events amplitudes and the temporal precision fish were continuously stimulated for 30 s at a given contrast.

Luminance sensitivity was assessed by stimulating the fish with a series of light steps (4 x 3 s) at 9 different light intensities increasing in steps of 0.5 log unit steps ranging from 11 pW mm^{-2} to 110 nW mm^{-2} (equivalent to 3.3 x 10^{11} photons mm^{-2}).

Drug injections

Dopamine signalling was manipulated by injecting the antagonist of D1 receptors SCH 23390 at a final estimated concentration of 200 nM (Sigma).Finally, the long-lasting dopamine receptor ligand [3H] 2-amino-6,7-dihydroxy 1,2,3,4-tetrahydronapthalene (ADTN) (Sigma) was injected to a final estimated concentration of 200 nM. We confirmed that these drugs gained access by including 1 mM Alexa 594 in the injection needle; within 5 mins of injection the dye could be detected within the inner plexiform layer of the retina. Vehicle injection did not affect synaptic responses to varying contrast.

Quantal decomposition of iGluSnFR signals.

To detect and quantize glutamatergic events from line-scans, there were six major steps, described in detail previously[23]. Steps 4-6 are summarized in Extended Data Figure 4.

1. Separation of regions of interest (ROIs) by spatial decomposition using Gaussian fits to the average intensity profile across the line-scan. Typically 1-3 hot-spots of iGluSnFR fluorescence were detected in a single terminal, representing active zones within the line-scan. Active zones more than 1-1.5 μm apart could be distinguished from eah other.

2. Time series extraction by weighted averaging. Once each spatial component had been defined, a time series for that component, F(t), was computed as the integral of the Gaussian fit to the linear intensity profile estimated in 1.

3. Baseline correction and calculation of ΔF/F. Bleaching sometimes occurred during an observation episode and was corrected using a linear function of time. The iGluSnFR signal used for all analyses was the relative change in fluorescence, ΔF/F0,

447 calculated from the bleach-corrected signals. The most frequent value (that is, the
448 baseline) of the trace was used as F0.
449
450 4. Identification of events by Wiener deconvolution. Release events within an active
451 zone were identified by their characteristic kinetics using a Wiener filter. The time-
452 course of iGluSnFR transients could be described by a function of the form:

453 $$\boldsymbol{h(t) = A * exp\left[-\frac{t}{\tau_f}\right] * \left(1 - exp\left[-\frac{t}{\tau_r}\right]\right)}, \quad (1)$$

454 where $\boldsymbol{A}$ describes the amplitude of the event and $\boldsymbol{\tau_r}$ and $\boldsymbol{\tau_f}$ and are the time constants
455 for rise and fall in the signal, respectively. Transients at most synapses could be
456 described using a kernel with parameters of $\boldsymbol{\tau_f}$ = 0.06 s and $\boldsymbol{\tau_r}$ = 0.001 s. These
457 parameters were relatively invariant for transients of different amplitudes so that
458 iGluSnFR transients could be described as a linear time-invariant system (LTI). The
459 filter described by equation 1 therefore allowed us to both "denoise" signals and
460 estimate the underlying input. The result of the Wiener deconvolution was a time series
461 in which glutamate release events were described approximately as Dirac-δ impulse.
462
463 5. Extraction of events. Although the use of Wiener deconvolution significantly
464 improved the signal-to-noise ratio, the baseline in the deconvolved traces was not
465 noiseless, making it necessary to set a threshold for counting a deviation in this signal
466 as an event. The distribution of values in the deconvolved trace was measured and
467 the threshold set at 3-4 standard deviations above the basline. Events were then
468 timed at the local maximum in the deconvolved trace above this threshold.
469
470 6. Amplitude clustering to create a time series of quantized events. A histogram of
471 event amplitudes at an individual active zone could be described as the sum of
472 Gaussians. The quantal amplitude, was then calculated as the average inter-peak
473 distance, which was always similar to the amplitude of the first peak, indicating that the

first peak in the distribution represents vesicles released individually. Based on the evidence that glutamate transients of varying amplitude were integer multiples of a unitary event or quantum, we partitioned events into numbers of quanta using a Gaussian Mixture Model (GMM). Under this framework, the probability **p** of a value **x** is given by:

$$\boldsymbol{p(x) = \sum_{i=1}^{K} \phi_i \mathcal{N}\left(x \middle| \mu_i, \sigma_i^2\right)} \quad (2)$$

where **N** is the normal probability density function and **Φ** represents the mixing probability and sums to one. We used the Expectation-Maximization (EM) algorithm for clustering and this was run up to 15 times on the synapse, each with a different number of components and with the mean and variance parameters initialized randomly, until acceptable convergence had been reached. Defining a time series as the number of quanta within each event allowed for computation of vesicle release rates and information theoretic measures.

Calculation of temporal jitter

In order to quantify variability in the timing of glutamatergic events, we first calculated the vector strength, r_q, for events composed of q quanta:

$$\boldsymbol{r_q = \frac{1}{N_q}\sqrt{\left(\sum_{i=1}^{N_q} cos\left(\frac{2\pi t_{q_i}}{T}\right)\right)^2 + \left(\sum_{i=1}^{N_q} sin\left(\frac{2\pi t_{q_i}}{T}\right)\right)^2}} \quad (3)$$

where t_{qi} is the time of the i^{th} q-quantal event, T is the stimulus period, and N_q is the total number of events of composed of q-quanta. The temporal jitter, J_q, can then be calculated as:

$$\boldsymbol{J_q = \frac{\sqrt{2(1 - r_q)}}{2\pi f}} \quad (4)$$

where f is the stimulus frequency.

498 **Calculations based on Information Theory**

499 To quantify the amount of information about a visual stimulus that is contained within
500 the sequence of release events from an active zone we first needed to convert
501 bipolar cell outputs into a probabilistic framework from which we could evaluate the
502 specific information (I_2), a metric that quantifies how much information about one
503 random variable is conveyed by the observation a specific symbol of another
504 random variable[41]. The time series of quantal events was converted into a
505 probability distribution by dividing into time bins of 20 ms, such that each bin
506 contained either zero events or one event of an integer amplitude. We then counted
507 the number of bins containing events of amplitude 1, or 2, or 3 etc. By dividing the
508 number of bins of each type by the total number of bins for each different stimulus,
509 we obtained the conditional distribution of **Q** given **S**, $p(\boldsymbol{Q}|\boldsymbol{S})$, where **Q** is the random
510 variable representing the *quanta/bin* and **S** is the random variable representing the
511 *stimulus contrasts* presented throughout the course of the experiment. In the
512 absence of information about the distribution of contrasts normally experienced by
513 a larval zebrafish, a uniform distribution of contrasts was used for S. Each contrast
514 step lasted 2 s (5 Hz) and they were presented in two different pseudo-random
515 orders, of which one is shown in Fig. 4D. The contrast sensitivity varied between
516 synapses and between morning and afternoon (Fig. 1E-G) so to make allowance
517 for this the stimulus set S was adjusted for each synapse to span contrasts ±10%
518 around $C_{1/2}$ measured within that synapse.

519 We computed the joint probability distribution by the chain rule for probability
520 (given the experimentally defined uniform distribution of stimuli **S**):

521 $$\boldsymbol{p}(\boldsymbol{S},\boldsymbol{Q}) = \boldsymbol{p}(\boldsymbol{Q}|\boldsymbol{S})\boldsymbol{p}(\boldsymbol{S}) \quad (\mathbf{5})$$

522 In order to convert this distribution into the conditional distribution of S given Q, we
523 used the definition of the conditional distribution:

524 $$\boldsymbol{p}(\boldsymbol{S}|\boldsymbol{Q}) = \frac{\boldsymbol{p}(\boldsymbol{S},\boldsymbol{Q})}{\boldsymbol{p}(\boldsymbol{Q})} \quad (\mathbf{6})$$

From these distributions we computed two metrics: the mutual information I(**S;Q**)[50] and specific information I_2(**S;q**) [44]. Mutual information is defined traditionally as:

$$\mathbf{I}(\boldsymbol{S};\boldsymbol{Q}) = \boldsymbol{H}(\boldsymbol{S}) - \boldsymbol{H}(\boldsymbol{S}|\boldsymbol{Q}) \quad (7)$$

$$\mathbf{I}(\boldsymbol{S};\boldsymbol{Q}) = \sum_{s\in S}\sum_{q\in Q} \boldsymbol{p}(s,q)\log_2\frac{\boldsymbol{p}(s)\boldsymbol{p}(q)}{\boldsymbol{p}(s,q)} = \boldsymbol{I}(\boldsymbol{Q};\boldsymbol{S}) \quad (8)$$

The specific information, I_2(**S;q**), is defined as the difference between the entropy of the stimulus S minus the conditional entropy of the stimulus given the observed symbol in the response q:

$$\boldsymbol{I_2}(\boldsymbol{S},\boldsymbol{q}) = \boldsymbol{H}(\boldsymbol{S}) - \boldsymbol{H}(\boldsymbol{S}|\boldsymbol{q}) \quad (9)$$

$$\boldsymbol{I_2}(\boldsymbol{S},\boldsymbol{q}) = -\sum_{s\in S}\boldsymbol{p}(s)\,\boldsymbol{log}\,\boldsymbol{p}(s) + \sum_{s\in S}\boldsymbol{p}(s|q)\,\boldsymbol{log}\,\boldsymbol{p}(s|q) \quad (10)$$

representing the amount of information observing each quantal event type q ϵ **Q** carries about the stimulus distribution **S**. Note that mutual information can also be computed from the specific information as the dot product of the specific information vector $\boldsymbol{I_2}$ and the vector describing the probability of an event of a given quantal size $\boldsymbol{p}(\boldsymbol{q})$. This adds to the interpretability of both metrics – the specific information is the amount of information a single (specific) symbol gives about the stimulus, and the mutual information is the average amount of information about the stimulus gained from observing any symbol.

Statistics

All data are given as mean ± s.e.m. unless otherwise stated in the figure legends. All statistical tests met appropriate assumptions and were calculated using inbuilt functions in IgorPro (Wavemetrics). When data were not normally distributed we used non-parametric tests. All tests were two-sided and significance defined as $P < 0.05$. Data collection was not randomized because all experiments were carried out within one set of animals. Delivery of different stimuli was randomized where appropriate. Data were only excluded from the analysis if the signal-to-noise ratio

(SNR) of the iGluSnFR signals elicited at a given synapse was not sufficient to detect unitary responses to visual stimuli with a SNR of at least three.

Acknowledgements

The authors express many thanks to all the members of Lagnado laboratory for discussions during the cours of this project. We also thank Tom Baden for his many insightful criticisms and suggestions. This work was supported by a grant to L.L. from the Wellcome Trust (102905/Z/13/Z).

Author contributions

J.M-D. conceived, designed and executed experiments, analyzed results and prepared the manuscript. B. J. carried out analysis and wrote code. F. E. conceived and executed experiments with SyGGCaM2 and carried out analysis. J. J. conceived and executed experiments and carried out analysis. L. L. conceived the project, designed experiments, analyzed data, repaired equipment, wrote code and prepared the manuscript.

Extended Data

Extended Data Figure 1

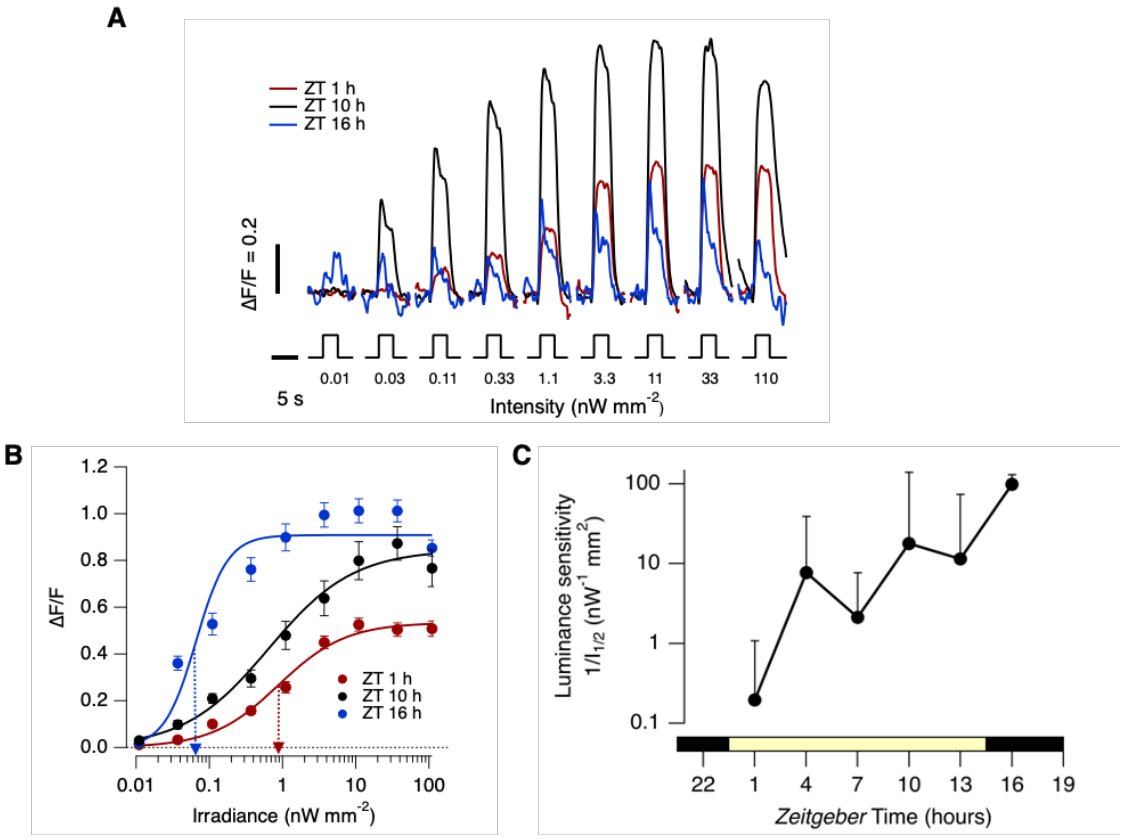

Extended Data Figure 1. Diurnal changes in luminance-sensitivity of bipolar cell synapses

A. Averaged responses from ON terminals to light steps of different irradiance measured at *Zeitgeber* time 1, 10 and 16 hours. Note large variations in amplitude and kinetics. Each light step was of 3 s (*n* = 535 terminals from 10 fish). **B.** Peak response as a function of irradiance for ON terminals in B. The smooth lines are Hill functions of the form $R = R_{max}*(I^h/(I^h + I_{1/2}^h))$, where R is the peak response, I is the irradiance, h is the Hill coefficient and $I_{1/2}$ is the irradiance generating the half-maximal response. At ZT = 16 hrs: R_{max} = 0.91 ± 0.04; h = 2.0 ± 0.2; $I_{1/2}$ = 0.066 ± 0.02 nW/mm^2 (dashed blue arrow). At ZT = 10 hrs: R_{max} = 0.85 ± 0.06; h = 0.8 ± 0.1; $I_{1/2}$ = 0.65 ± 0.18 nW/mm^2. At ZT = 1 hrs: R_{max} = 0.853 ± 0.02; h = 0.9 ± 0.2; $I_{1/2}$ = 0.88 ± 0.18 nW/mm^2 (red arrow). **C.** Variations in luminance sensitivity as a function of *Zeitgeber* time averaged across both ON and OFF terminals (n=535 and 335, respectively). The lower bar shows the timing of the light-dark cycle.

Extended Data Figure 2

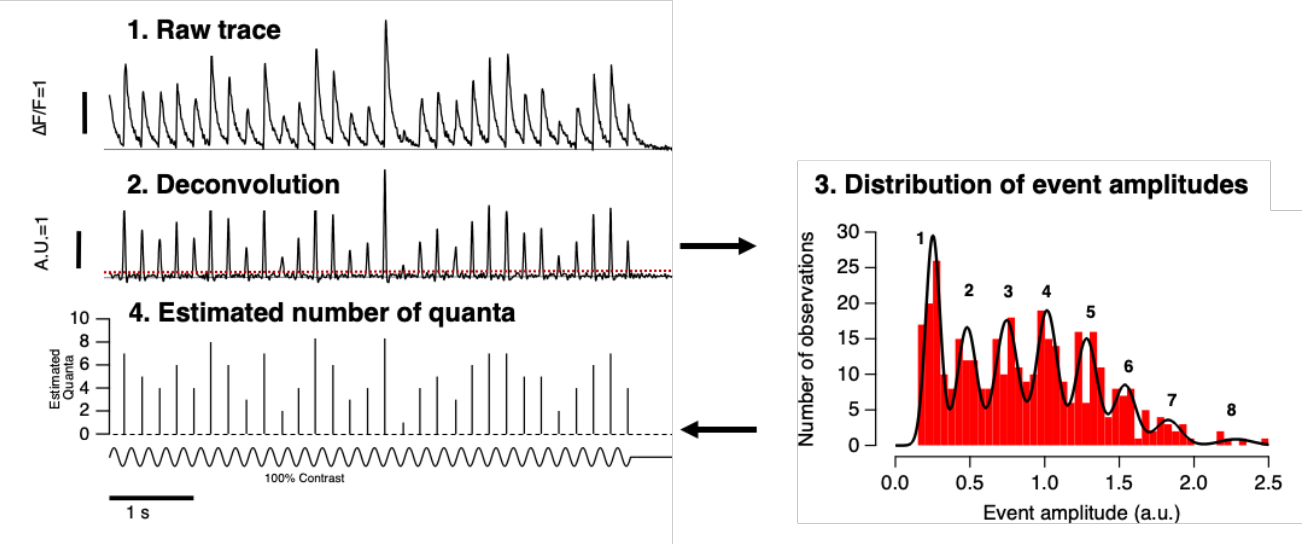

Extended Data Figure 2. Decomposition of iGluSnFR signals into vesicle counts

Summary of the basic steps for quantal decomposition of iGluSnFr signals. ***1.*** Raw trace extracted from individual active zones (linescan, 1 KHz). ***2.*** Deconvolved trace using the estimated Wiener filter. The dashed red line shows the threshold for counting evebts above the noise. ***3.*** Histogram of event amplitudes for a representative active zone (373 events accumulated using stimulus contrasts of 20%, 60% and 100% and a frequency of 5 Hz). The black line is a fit of eight Gaussians, identified using a Gaussian mixture model. Note that the variance of successive Gaussians did not increase in proportion to the peak number. The first peak had a value of 0.24, and the distance between peaks averaged 0.25, indicating the existence of a quantal event equivalent to ~0.25. ***4.*** Estimation of the number of quanta per event. For more details about analyses see James et al., 2019.

Extended Data Figure 3

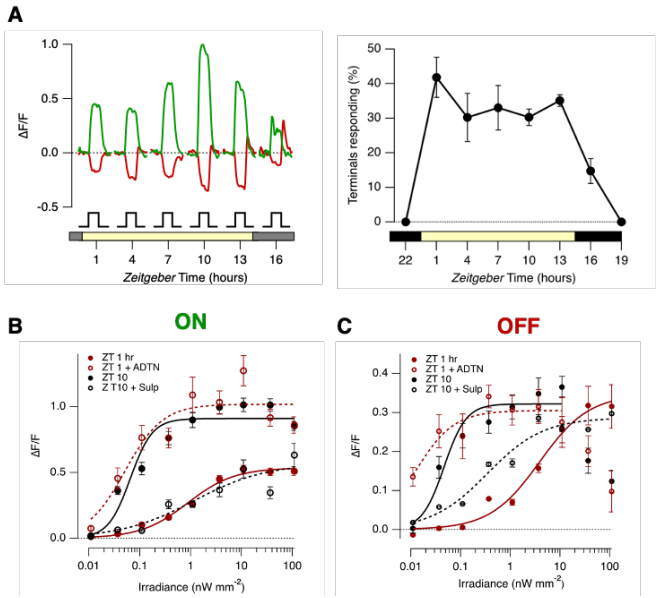

Extended Data Figure 3. Diurnal changes in luminance sensitivity

A. Left: Averaged SyGaMP2 signals at different *Zeitgeber* time. ON terminals green and OFF terminas red. Each step of light (10 nW mm^{-2}) lasted 3 s. These averages are only from responsive terminals. Right: the percentage of terminals generating a significant response to the same light step (averaged across both ON and OFF). Bars show SD. **B.** Effects of manipulating dopamine signalling on luminance sensitivity of the ON channel. Luminance vs. response plots for ON terminals. Red circles compare this function at ZT 1 hr under control conditions (solid circle) and after injection of the non-selective dopamine receptor agonist ADTN (~0.2 µM; open circles). ADTN caused a prompt change in the luminance-response function to forms measured at ZT 10 hrs (solid black circles), increasing R_{max} from 0.53 ± 0.02 to 1.02 ± 0.07, and reducing $I_{1/2}$ from 0.88 ± 0.18 nW mm^{-2} to 0.05 ± 0.02 nW mm^{-2} (± sd, as estimated from the fitted Hill function shown). The higher gain and luminance sensitivity at ZT 10 hrs could be explained as an effect of dopamine at D2 receptors, because it was completely reversed by injection of the selective D2 receptor antagonist sulpiride (~2 µM; open black circles; R_{max} = 0.57 ± 0.13, $I_{1/2}$ = 1.16 ± 1.34 nW mm^{-2}). Results collected from *n* = 535 terminals from 38 fish. **C.** Effects of manipulating dopamine signalling on luminance sensitivity of the OFF channel. Comparing control responses at ZT 1 hr and 10 hrs showed a significant reduction in $I_{1/2}$ from 3.9 ± 1.3 to 0.0128 ± 0.005, but *without* a significant change in R_{max} (0.35 ± 0.03 vs 0.30 ± 0.02). ADTN injected at ZT 1 caused a prompt increase in luminance sensitivity, reducing $I_{1/2}$ to 0.013 ± 0.005 nW mm^{-2}. The higher luminance sensitivity at ZT 10 hrs could be partly explained as an effect of dopamine at D2 receptors, because injection of sulpiride (~2 µM; open black circles) increased $I_{1/2}$ from 0.05 ± 0.01 nW mm^{-2} to 0.35 ± 0.14 nW mm^{-2}. Results collected from *n* = 355 terminals from 38 fish.

References

1 Bargmann, C. I. & Marder, E. From the connectome to brain function. *Nat Methods* **10**, 483-490, doi:nmeth.2451 [pii] 10.1038/nmeth.2451 (2013).

2 McCormick, D. A., Nestvogel, D. B. & He, B. J. Neuromodulation of brain state and behavior. *Annual review of neuroscience* **43**, 391-415 (2020).

3 Nadim, F. & Bucher, D. Neuromodulation of neurons and synapses. *Current opinion in neurobiology* **29**, 48-56, doi:10.1016/j.conb.2014.05.003 (2014).

4 Patzke, C. *et al.* Neuromodulator signaling bidirectionally controls vesicle numbers in human synapses. *Cell* **179**, 498-513. e422 (2019).

5 Rusakov, D. A., Savtchenko, L. P. & Latham, P. E. Noisy Synaptic Conductance: Bug or a Feature? *Trends Neurosci* **43**, 363-372, doi:10.1016/j.tins.2020.03.009 (2020).

6 Euler, T., Haverkamp, S., Schubert, T. & Baden, T. Retinal bipolar cells: elementary building blocks of vision. *Nat Rev Neurosci* **15**, 507-519, doi:10.1038/nrn3783 (2014).

7 Wadiche, J. I. & Jahr, C. E. Multivesicular release at climbing fiber-Purkinje cell synapses. *Neuron* **32**, 301-313 (2001).

8 Glowatzki, E. & Fuchs, P. A. Transmitter release at the hair cell ribbon synapse. *Nat Neurosci* **5**, 147-154, doi:10.1038/nn796 (2002).

9 Christie, J. M. & Jahr, C. E. Multivesicular release at Schaffer collateral-CA1 hippocampal synapses. *The Journal of neuroscience : the official journal of the Society for Neuroscience* **26**, 210-216, doi:10.1523/JNEUROSCI.4307-05.2006 (2006).

10 Higley, M. J., Soler-Llavina, G. J. & Sabatini, B. L. Cholinergic modulation of multivesicular release regulates striatal synaptic potency and integration. *Nature neuroscience* **12**, 1121-1128 (2009).

11 Holler, S., Köstinger, G., Martin, K. A. C., Schuhknecht, G. F. P. & Stratford, K. J. Structure and function of a neocortical synapse. *Nature* **591**, 111-116, doi:10.1038/s41586-020-03134-2 (2021).

12 Ribelayga, C., Cao, Y. & Mangel, S. C. The circadian clock in the retina controls rod-cone coupling. *Neuron* **59**, 790-801, doi:10.1016/j.neuron.2008.07.017 (2008).

13 Nie, K. *et al.* Effects of circadian clock protein Per1b on zebrafish visual functions. *Chronobiology international* **35**, 160-168 (2018).

14 Li, L. Circadian Vision in Zebrafish: From Molecule to Cell and from Neural Network to Behavior. *J Biol Rhythms* **34**, 451-462, doi:10.1177/0748730419863917 (2019).

15 Zang, J. *et al.* Circadian Regulation of Vertebrate Cone Photoreceptor Function. *bioRxiv*, 2021.2005.2005.442714, doi:10.1101/2021.05.05.442714 (2021).

16 Nikolaev, A., Leung, K. M., Odermatt, B. & Lagnado, L. Synaptic mechanisms of adaptation and sensitization in the retina. *Nat Neurosci* **16**, 934-941, doi:10.1038/nn.3408 (2013).

17 Zimmermann, M. J. Y. *et al.* Zebrafish Differentially Process Color across Visual Space to Match Natural Scenes. *Curr Biol* **28**, 2018-2032.e2015, doi:10.1016/j.cub.2018.04.075 (2018).

18 Franke, K. *et al.* Inhibition decorrelates visual feature representations in the inner retina. *Nature* **542**, 439-444, doi:10.1038/nature21394 (2017).

19 Johnston, J. *et al.* A Retinal Circuit Generating a Dynamic Predictive Code for Oriented Features. *Neuron* **102**, 1211-1222 e1213, doi:10.1016/j.neuron.2019.04.002 (2019).

20 Matsumoto, A. *et al.* Direction selectivity in retinal bipolar cell axon terminals. *Neuron* (2021).

21 Lagnado, L. & Schmitz, F. Ribbon Synapses and Visual Processing in the Retina. *Annu Rev Vis Sci* **1**, 235-262, doi:10.1146/annurev-vision-082114-035709 (2015).

22 Singer, J. H., Lassova, L., Vardi, N. & Diamond, J. S. Coordinated multivesicular release at a mammalian ribbon synapse. *Nat Neurosci* **7**, 826-833, doi:10.1038/nn1280 (2004).

23 James, B., Darnet, L., Moya-Diaz, J., Seibel, S. H. & Lagnado, L. An amplitude code transmits information at a visual synapse. *Nat Neurosci* **22**, 1140-1147, doi:10.1038/s41593-019-0403-6 (2019).

24 Auger, C., Kondo, S. & Marty, A. Multivesicular release at single functional synaptic sites in cerebellar stellate and basket cells. *The Journal of neuroscience : the official journal of the Society for Neuroscience* **18**, 4532-4547 (1998).

25 Dreosti, E., Odermatt, B., Dorostkar, M. M. & Lagnado, L. A genetically encoded reporter of synaptic activity in vivo. *Nat Methods* **6**, 883-889, doi:10.1038/nmeth.1399 (2009).

26 Marvin, J. S. *et al.* An optimized fluorescent probe for visualizing glutamate neurotransmission. *Nat Methods* **10**, 162-170, doi:10.1038/nmeth.2333 (2013).

27 Jackson, C. R. *et al.* Retinal dopamine mediates multiple dimensions of light-adapted vision. *The Journal of neuroscience : the official journal of the Society for Neuroscience* **32**, 9359-9368, doi:10.1523/JNEUROSCI.0711-12.2012 (2012).

28 Esposti, F., Johnston, J., Rosa, J. M., Leung, K. M. & Lagnado, L. Olfactory stimulation selectively modulates the OFF pathway in the retina of zebrafish. *Neuron* **79**, 97-110, doi:10.1016/j.neuron.2013.05.001 (2013).

29 Roy, S. & Field, G. D. Dopaminergic modulation of retinal processing from starlight to sunlight. *J Pharmacol Sci* **140**, 86-93, doi:10.1016/j.jphs.2019.03.006 (2019).

30 Shannon, C. A Mathematical Theory of Communication. *Bell System Technical Journal* **27**, 379-423 (1948).

31 Faisal, A. A., Selen, L. P. & Wolpert, D. M. Noise in the nervous system. *Nat Rev Neurosci* **9**, 292-303, doi:10.1038/nrn2258 (2008).

712 32 London, M., Roth, A., Beeren, L., Hausser, M. & Latham, P. E. Sensitivity to
713 perturbations in vivo implies high noise and suggests rate coding in cortex. *Nature* **466**,
714 123-127, doi:10.1038/nature09086 (2010).

715 33 Churchland, M. M. *et al.* Stimulus onset quenches neural variability: a widespread
716 cortical phenomenon. *Nature Neuroscience* **13**, 369-378, doi:10.1038/nn.2501 (2010).

717 34 Fairhall, A. L. Whither variability? *Nature Neuroscience* **22**, 329-330,
718 doi:10.1038/s41593-019-0344-0 (2019).

719 35 Berry, M. J., Warland, D. K. & Meister, M. The structure and precision of retinal
720 spike trains. *Proceedings of the National Academy of Sciences* **94**, 5411,
721 doi:10.1073/pnas.94.10.5411 (1997).

722 36 Rathbun, D. L., Warland, D. K. & Usrey, W. M. Spike timing and information
723 transmission at retinogeniculate synapses. *Journal of Neuroscience* **30**, 13558-13566
724 (2010).

725 37 Cui, Y., Wang, Y. V., Park, S. J. H., Demb, J. B. & Butts, D. A. Divisive suppression
726 explains high-precision firing and contrast adaptation in retinal ganglion cells. *eLife* **5**,
727 e19460, doi:10.7554/eLife.19460 (2016).

728 38 Freed, M. A. Quantal encoding of information in a retinal ganglion cell. *J*
729 *Neurophysiol* **94**, 1048-1056, doi:10.1152/jn.01276.2004 (2005).

730 39 Choi, S. Y. *et al.* Encoding light intensity by the cone photoreceptor synapse.
731 *Neuron* **48**, 555-562, doi:10.1016/j.neuron.2005.09.011 (2005).

732 40 Odermatt, B., Nikolaev, A. & Lagnado, L. Encoding of luminance and contrast by
733 linear and nonlinear synapses in the retina. *Neuron* **73**, 758-773,
734 doi:10.1016/j.neuron.2011.12.023 (2012).

735 41 Stone, J. V. *Principles of Neural Information Theory: Computational Neuroscience*
736 *and Metabolic Efficiency* (Sebtel Press, 2018).

737 42 Schultz, S. R. Signal-to-noise ratio in neuroscience. *Scholarpedia* **2**, 2046 (2007).

738 43 Borst, A. & Theunissen, F. E. Information theory and neural coding. *Nat Neurosci*
739 **2**, 947-957, doi:10.1038/14731 (1999).

740 44 DeWeese, M. R. & Meister, M. How to measure the information gained from one
741 symbol. *Network* **10**, 325-340 (1999).

742 45 Laughlin, S. B. Energy as a constraint on the coding and processing of sensory
743 information. *Curr Opin Neurobiol* **11**, 475-480, doi:10.1016/s0959-4388(00)00237-3
744 (2001).

745 46 Koch, K. *et al.* How much the eye tells the brain. *Curr Biol* **16**, 1428-1434,
746 doi:10.1016/j.cub.2006.05.056 (2006).

747 47 Oertner, T. G., Sabatini, B. L., Nimchinsky, E. A. & Svoboda, K. Facilitation at
748 single synapses probed with optical quantal analysis. *Nature neuroscience* **5**, 657-664
749 (2002).

48 Chalifoux, J. R. & Carter, A. G. GABAB receptors modulate NMDA receptor calcium signals in dendritic spines. *Neuron* **66**, 101-113 (2010).

49 Pologruto, T. A., Sabatini, B. L. & Svoboda, K. ScanImage: flexible software for operating laser scanning microscopes. *Biomed Eng Online* **2**, 13, doi:10.1186/1475-925X-2-13 (2003).

50 de Ruyter van Steveninck, R. R., Lewen, G. D., Strong, S. P., Koberle, R. & Bialek, W. Reproducibility and variability in neural spike trains. *Science* **275**, 1805-1808, doi:10.1126/science.275.5307.1805 (1997).

51 Pola, G., Schultz, S. R, Petersen, R. S & Panzeri, S. in *Neuroscience Databases: A Practical Guide* (Springer, Boston, MA, 2003).